Int. J. Engng Sci. Vol. 31, No. 4, pp. 529–547, 1993
Printed in Great Britain.
0020-7225/93 \$6.00 + 0.00

ANALYSIS OF SHEAR BANDS IN DYNAMIC AXISYMMETRIC COMPRESSION OF A THERMOVISCOPLASTIC CYLINDER

R. C. BATRA and K. I. KO
Department of Mechanical and Aerospace Engineering and Engineering Mechanics, University of Missouri-Rolla, Rolla, MO 65401-0249, U.S.A.

Abstract—We study dynamic axisymmetric thermomechanical deformations of a viscoplastic cylinder with its boundaries assumed to be thermally insulated, its mantle traction free, and its top and bottom surfaces compressed at a prescribed rate. We consider two limiting cases of the frictional force between the loading device and the cylinder, i.e. either there is no sliding between the two surfaces, or there is smooth contact. It is found that the shear bands initiate much later when frictional force is neglected than when it is considered. A comparison of the presently computed results with those for the case when the body is assumed to be deformed in plane strain compression reveals that the initiation of shear bands is delayed significantly for the axisymmetric problem.

1. INTRODUCTION

Zener and Hollomon [1] observed 32 μm wide shear bands during the punching of a hole in a low carbon steel plate, and postulated that heating caused by the plastic deformation of the material made it softer and the material became unstable when this thermal softening equalled the combined effects of strain and strain-rate hardening. Subsequent experimental [2, 3] and numerical [4–6] studies have revealed that shear bands generally form at an average strain much more than the one when the shear stress or the effective stress attains its peak value. Backman and Finnegan [7] have pointed out that shear bands initiate from flaws, second phase particles, or other material defects present in the body and propagate like a crack. The analytical and numerical studies have modeled a material defect by introducing (i) a perturbation in temperature or strain-rate, (ii) a geometric imperfection such as a notch or a smooth variation in the thickness of the specimen, (iii) a weak material at the site of the defect, (iv) a void, or (v) a rigid inclusion. Batra [6] studied simple shearing deformations of a viscoplastic body and found that large temperature perturbations caused the shear bands to initiate at an average strain less than the one when the shear stress attained its peak value in a defect-free body.

Wulf [8] tested 7039 aluminum cylinders in compression at average strain-rates of 2000–25,000 s^{-1} and observed that circular cross-sections were deformed into elliptical ones, and shear bands formed in specimens which subsequently failed by crack propagation along the dominant band. Here we study the dynamic thermomechanical deformations of an isotropic circular steel cylinder deformed in compression at a nominal strain-rate of 5000 s^{-1}, and model a material defect by introducing a temperature perturbation at the center of the cylinder. We assume that the deformations of the cylinder are axisymmetric even after a shear band has formed. There is no fracture or failure criterion included in our work; thus, the cylinder can undergo unlimited deformations. The computed results show that shear bands form much later when the contact surfaces between the loading device and the ends of the cylinder are modeled as smooth than when they are taken to be sticking with each other. A comparison of the present results with those when the body is assumed to deform in plane strain compression reveals that the initiation of shear bands is delayed considerably in a body undergoing axisymmetric deformations.

2. FORMULATION OF THE PROBLEM

A schematic sketch of the problem studied is shown in Fig. 1. We use cylindrical coordinates with origin at the center of the cylinder to analyze its axisymmetric deformations, presume that

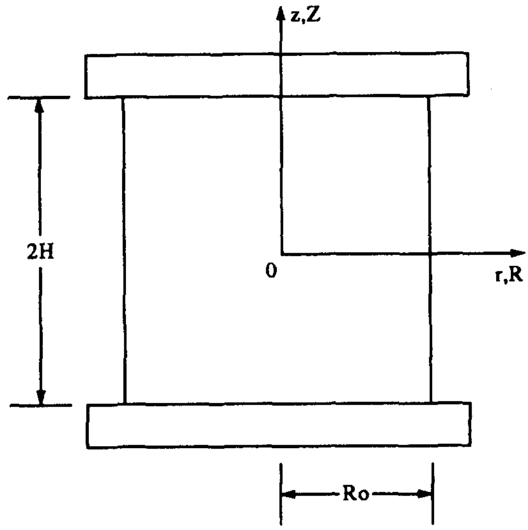

Fig. 1. A schematic sketch of the problem studied.

it is made of a thermally softening viscoplastic material, and is loaded at its ends by an impulsive load. Because of the symmetry of deformations about the horizontal centroidal plane, we analyze deformations of the upper half of the cylinder. In terms of the Lagrangian description of motion, equations governing the thermomechanical deformations of the body are

$$(\rho J)^{\cdot} = 0, \tag{1}$$

$$\rho_0 \dot{\mathbf{v}} = \operatorname{Div} \mathbf{T}, \tag{2}$$

$$\rho_0 \dot{\mathbf{e}} = -\operatorname{Div} \mathbf{Q} + \mathbf{T}\colon \operatorname{Grad} \mathbf{v}, \tag{3}$$

$$\mathbf{T} = \frac{\rho_0}{\rho} \boldsymbol{\sigma} \mathbf{F}^{-T}, \qquad \boldsymbol{\sigma} = -B\left(\frac{\rho}{\rho_0} - 1\right)\mathbf{1} + 2\mu \mathbf{D}, \tag{4}$$

$$2\mu = \frac{\sigma_0}{\sqrt{3}\, I}(1 + bI)^m (1 - \nu\theta), \tag{5}$$

$$\mathbf{Q} = \frac{\rho_0}{\rho} \mathbf{F}^{-1} \mathbf{q}, \qquad \mathbf{q} = -k \operatorname{grad} \theta, \tag{6}$$

$$2\mathbf{D} = \operatorname{grad} \mathbf{v} + (\operatorname{grad} \mathbf{v})^T, \qquad 2I^2 = \hat{\mathbf{D}}:\hat{\mathbf{D}}, \qquad \hat{\mathbf{D}} = \mathbf{D} - \frac{1}{3}(\operatorname{tr} \mathbf{D})\mathbf{1}, \tag{7}$$

$$\dot{e} = c\dot{\theta} + \dot{\rho} B\left(\frac{\rho}{\rho_0} - 1\right)\Big/(\rho\rho_0), \qquad J = \det \mathbf{F}, \qquad \mathbf{F} = \operatorname{Grad} \mathbf{x}. \tag{8}$$

Equations (1), (2), and (3) express, respectively, the balance of mass, balance of linear momentum, and the balance of internal energy; equations $(4)_2$, $(6)_2$, and $(8)_1$ are, respectively, the presumed constitutive relations for the Cauchy stress $\boldsymbol{\sigma}$, heat flux $\mathbf{q}$ measured per unit area in the present or deformed configuration, and the rate of change of the specific internal energy e. In equations (1)–(8), ρ is the present mass density, ρ_0 the mass density in the reference configuration, $\mathbf{v}$ the velocity of a material particle, the operators Div and Grad signify the divergence and the gradient operations in the reference configuration, the operator grad is the gradient of a quantity in the present configuration, $\mathbf{A}:\mathbf{B}$ equals $\operatorname{tr}(\mathbf{A}\mathbf{B}^T)$ for second order tensors $\mathbf{A}$ and $\mathbf{B}$, and a superimposed dot indicates the material time derivative. Furthermore, $\mathbf{F}$ is the deformation gradient, $\mathbf{D}$ the strain-rate tensor, $\hat{\mathbf{D}}$ the deviatoric strain-rate tensor, $\mathbf{x}$ gives the present location of a material particle that occupied place $\mathbf{X}$ in the reference configuration, $\mathbf{T}$ the first Piola–Kirchhoff stress tensor, $\mathbf{Q}$ the heat flux measured per unit area in the reference configuration, θ the temperature rise, σ_0 is the yield stress in a quasistatic simple compression test, B is the bulk modulus, parameters b and m describe the strain-rate hardening of the material, ν characterizes its thermal softening, k its thermal conductivity, and c the specific heat. Defining the deviatoric stress tensor $\mathbf{s}$ by

$$\mathbf{s} = \boldsymbol{\sigma} + B\left(\frac{\rho}{\rho_0} - 1\right)\mathbf{1} - \frac{2\mu}{3}(\operatorname{tr}\mathbf{D})\mathbf{1} = 2\mu\hat{\mathbf{D}}, \tag{9}$$

we get

$$\left(\frac{1}{2}\operatorname{tr}(\mathbf{s}\mathbf{s}^T)\right)^{1/2} = \frac{\sigma_0}{\sqrt{3}}(1 - \nu\theta)(1 + bI)^m. \tag{10}$$

The constitutive relation $(4)_2$ with μ given by (5) generalizes the one proposed by Litonski [9] for simple shearing deformations of the material. Batra [10] proposed and used equation $(4)_2$ to study the steady-state axisymmetric deformations of a thermoviscoplastic target being penetrated by a fast moving rigid cylindrical rod, and it has been referred to as the Litonski–Batra flow rule. Batra and Jayachandran [11] have shown that the Litonski–Batra flow rule and those proposed by Bodner and Partom [12] and Brown *et al.* [13], when calibrated against a hypothetical compression test and subsequently used to study the axisymmetric steady-state penetration problem, predict essentially identical patterns of target deformations. We note that Bell [14], Lin and Wagoner [15], and Lindholm and Johnson [16] concluded from their test results that the flow stress decreases linearly with the temperature rise for the materials they tested.

We introduce nondimensional variables, indicated below by a superimposed bar, as follows:

$$\bar{\boldsymbol{\sigma}} = \boldsymbol{\sigma}/\sigma_0, \quad \bar{\mathbf{s}} = \mathbf{s}/\sigma_0, \quad \bar{B} = B/\sigma_0, \quad \bar{\mathbf{T}} = \mathbf{T}/\sigma_0, \quad \bar{\mathbf{v}} = \mathbf{v}/v_0, \quad \bar{t} = tv_0/H,$$
$$\bar{\mathbf{x}} = \mathbf{x}/R_0, \quad \bar{\theta} = \theta/\theta_0, \quad \bar{b} = b(v_0/H), \quad \bar{\nu} = \nu\theta_0, \quad \bar{\rho} = \rho/\rho_0,$$
$$\theta_0 \equiv \sigma_0/(\rho_0 c), \quad \bar{\mathbf{D}} = \mathbf{D}H/v_0, \quad \bar{I} = IH/v_0. \tag{11}$$

Here $2H$ is the height of the cylinder, R_0 its radius, and v_0 the imposed speed on the top and bottom surfaces. Henceforth we use nondimensional variables and drop the superimposed bars.

We study only axisymmetric deformations of the viscoplastic cylinder, and presume that they are symmetric about the horizontal centroidal plane. Pertinent boundary conditions for the material in the first quadrant of the R–Z plane are:

$$v_r = 0, \quad T_{zR} = 0, \quad Q_R = 0 \quad \text{on the axis of symmetry} \quad r = R = 0,$$
$$v_z = 0, \quad T_{rZ} = 0, \quad Q_Z = 0 \quad \text{on} \quad z = Z = 0,$$
$$T_{rR} = 0, \quad T_{zR} = 0, \quad Q_R = 0 \quad \text{on the mantle of the cylinder } r = R_0,$$
$$v_z = -U(t), \quad Q_Z = 0 \quad \text{and either } T_{rZ} = 0 \text{ or } v_r = 0, \text{ on the top surface} \quad Z = H. \tag{12}$$

That is, boundary conditions resulting from the presumed symmetry of deformations are applied on the left and bottom faces, the mantle of the cylinder is taken to be traction free, normal velocity is prescribed on the top surface, and either zero radial velocity or zero tangential traction is applied on the top surface, which simulates the condition of no sliding or no frictional force acting between the loading device and the cylinder surface. All bounding surfaces of the cylinder are presumed to be thermally insulated from the surroundings. We take the function $U(t)$ as

$$\begin{aligned} U(t) &= t/0.005, && 0 \le t \le 0.005, \\ &= 1, && t \ge 0.005, \end{aligned} \tag{13}$$

and the initial conditions as

$$\rho(R, Z, 0) = 1.0, \qquad \mathbf{v}(R, Z, 0) = \mathbf{0},$$
$$\theta(R, Z, 0) = \epsilon(1 - \delta^2)^9 \exp(-5\delta^2), \qquad \delta^2 = R^2 + Z^2. \tag{14}$$

Thus the block is initially at rest, has a uniform mass density, but nonuniform temperature which is high at the origin and rapidly falls off to zero as we move away from it. The initial temperature $(14)_3$ models a material defect and its magnitude ϵ at the origin represents in some sense the strength of the defect.

3. BRIEF DESCRIPTION OF THE SOLUTION TECHNIQUE

The problem formulated above is highly nonlinear and too complicated to solve analytically. It is difficult, if not impossible, to prove an existence and/or a uniqueness theorem for it. Here we seek an approximate solution of the problem numerically by the finite element method, and use an updated Lagrangian description of motion. That is, to find the deformed configuration of the body at time $(t + \Delta t)$ we take its configuration at time t as the reference configuration. However, the deformations during this time interval Δt may be finite. We first reduce the coupled nonlinear partial differential equations governing the thermomechanical deformations of the body to a set of coupled, nonlinear, and ordinary stiff differential equations by using the Galerkin approximation. A finite element mesh consisting of 3-noded triangular elements with 3-point quadrature rule and lumped mass matrix, obtained by the row-sum technique, is used. At each node point of the finite element mesh, two components of the velocity, the temperature and the mass density, are taken as unknowns. The stiff ordinary differential equations are integrated with respect to time by using the backward difference Adam's method included in the subroutine LSODE developed by Hindmarsh [17]. The Gear method, also included in LSODE, could not be used because of the limited core storage available.

We delineate narrow regions of intense plastic deformation by using an adaptive mesh refinement technique developed by Batra and Ko [18] and described in the Appendix. After having obtained solution for a few time steps with a coarse mesh, the mesh is refined so that the integral of the second invariant of the strain-rate tensor over each element is essentially the same. Thus, smaller elements are generated in regions where the material is deforming severely, and coarser elements elsewhere.

4. COMPUTATION AND DISCUSSION OF RESULTS

Assuming that the cylinder is made of a typical steel, we assigned the following values to various material and geometric parameters.

$$b = 10{,}000\,\mathrm{s}, \qquad \sigma_0 = 333\,\mathrm{MPa}, \qquad k = 49.2\,\mathrm{Wm^{-1}{}^\circ C^{-1}}, \qquad m = 0.025,$$
$$c = 473\,\mathrm{Jkg^{-1}{}^\circ C^{-1}}, \qquad \rho_0 = 7800\,\mathrm{kg\,m^{-3}}, \qquad B = 128\,\mathrm{GPa},$$
$$\nu = 0.0222\,{}^\circ\mathrm{C}^{-1}, \qquad v_0 = 25\,\mathrm{m\,s^{-1}}, \qquad H = R_0 = 5.0\,\mathrm{mm}, \qquad \epsilon = 0.2. \tag{15}$$

We have stated dimensional quantities to clarify the units used. Thus, the cylinder is compressed at an average strain-rate of $5000\,\mathrm{s}^{-1}$. For values given in (15), $\theta_0 = 89.6°\mathrm{C}$, and the nondimensional melting temperature θ_m defined as $1/\nu$ equals 0.5027. We have taken a rather large value of the thermal softening coefficient ν so as to reduce the computational time. It should not affect the qualitative nature of results. In view of the lack of test data in a shear band, and the unavailability of detailed information about the evolution of a shear band in a compression problem, one can only see whether or not computed results predict well qualitatively various aspects of the shear band formation.

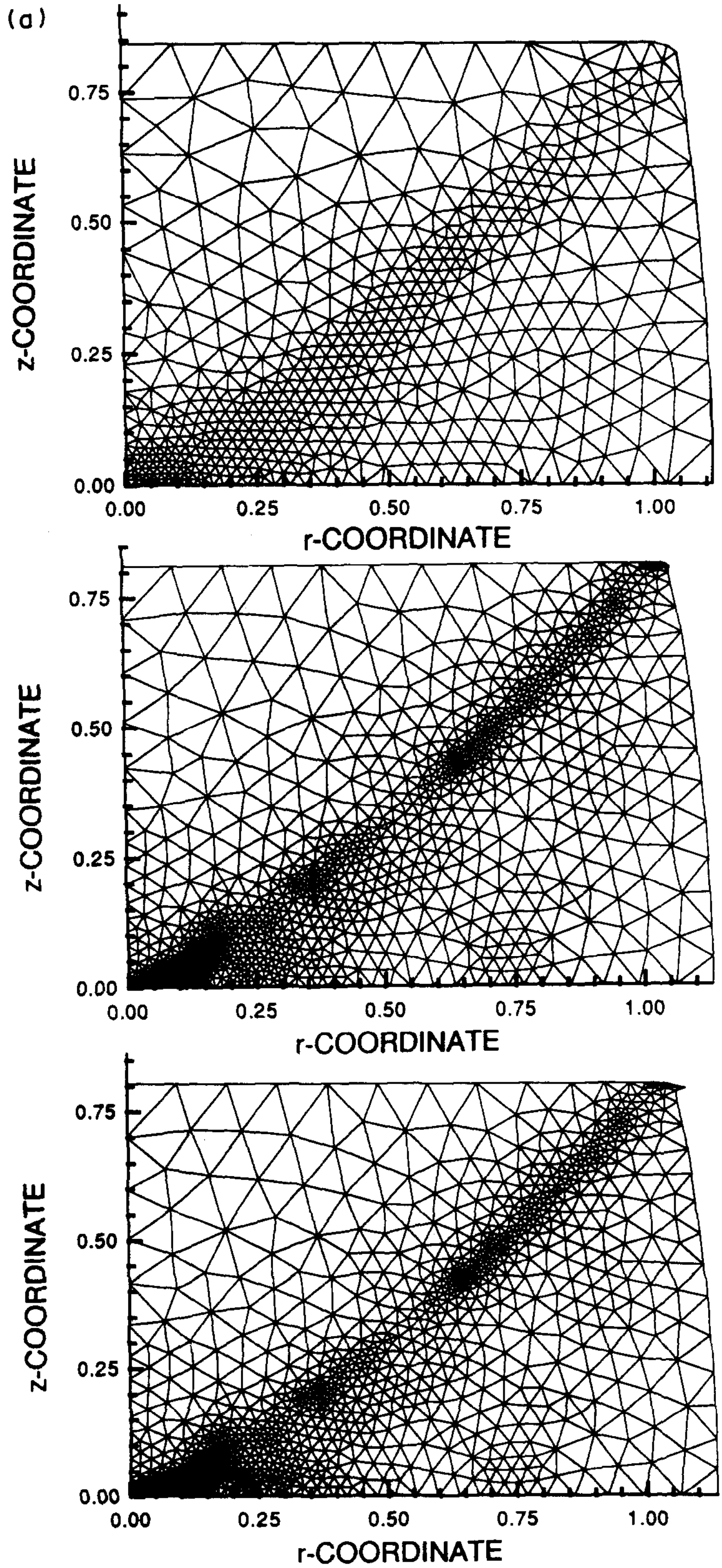

Fig. 2.—(*Caption overleaf*).

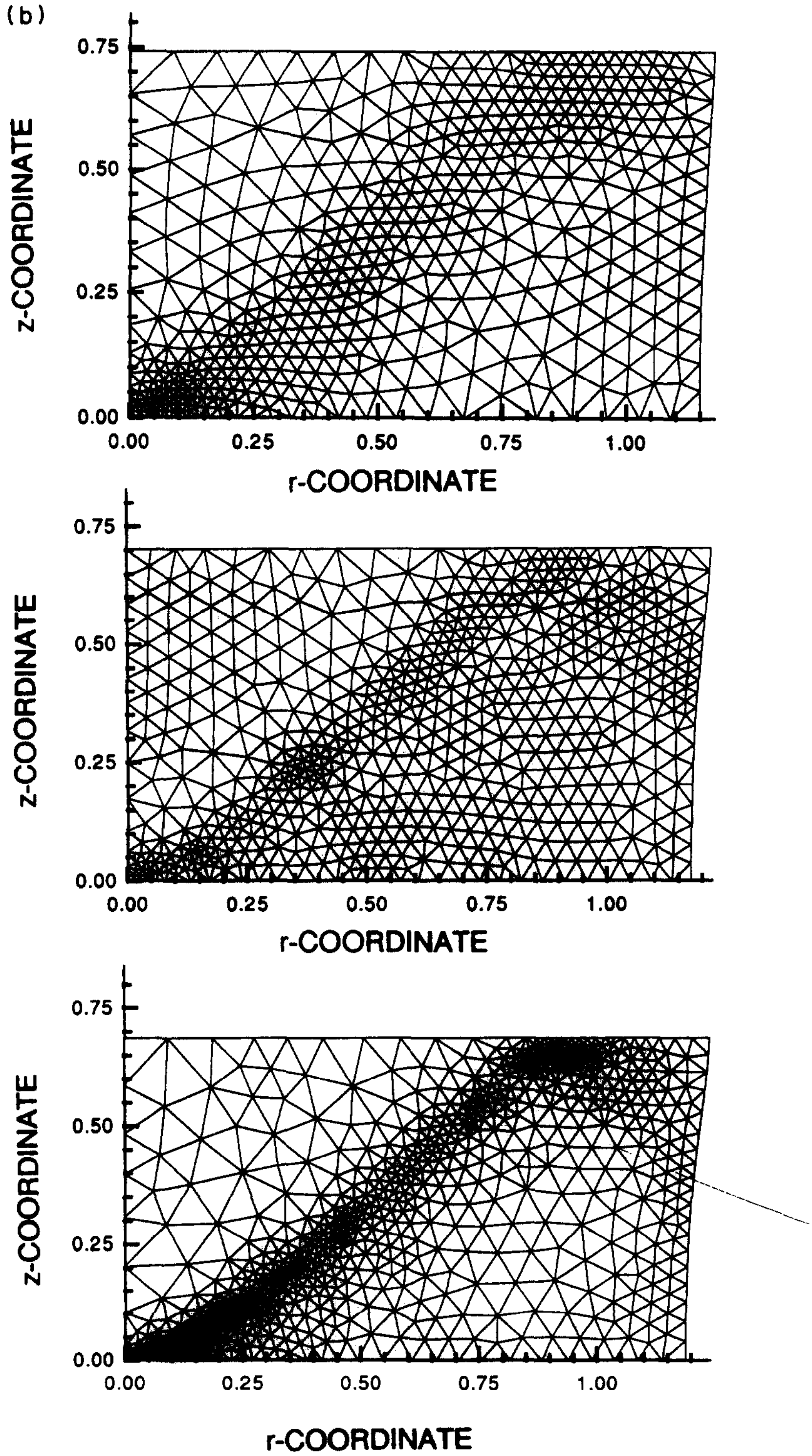

Fig. 2. (a) Refined finite element meshes at nondimensional times $t = 0.160$, 0.190, and 0.197 for the no slipping case; (b) $t = 0.26$, 0.30, and 0.315 for the case of the smooth contact.

The finite element mesh at time $t = 0$ had 400 uniform triangular elements with 441 nodes. The mesh was refined when the second invariant I of the deviatoric strain-rate tensor at the origin equalled 5, and subsequently for every increment of 0.01 in the nondimensional temperature θ at the specimen center. The finite element meshes so generated in the configurations at time $t = 0.160$, 0.190, and 0.197 when there is no slipping allowed at the contact surface between the loading device and the cylinder ends are depicted in Fig. 2(a). These plots discern the barrelling effect observed in compression tests, and also the severely deforming narrow region. The strain-rate near the top right corner is very high, too, and the elements there are deformed significantly. However, such is not the case when the contact surfaces between the loading device and cylinder ends are taken to be smooth. This is clear from the plots of the finite element meshes generated at time $t = 0.26$, 0.30, and 0.315 given in Fig. 2(b). In this case, the lateral displacement of material particles on the end faces is more than that of the similarly situated particles on the centroidal horizontal plane, and there is the reversed barrelling effect. This reversed barrelling was observed by Wulf [19] in high strain-rate compression of titanium and some titanium alloys, who used graphite grease to hold the specimens and also as a lubricant. Even though the average strain in the cylinder is more than that with the no slipping case, the deformations appear to be less intense within the band. This is mainly due to the differences in the deformations of the region near the top right corner for the two cases. To elucidate this, we have plotted in Fig. 3 the evolution of the second invariant I of the deviatoric strain-rate tensor at the top right corner. These plots indicate that the region near the top right corner deforms severely when the loading device is assumed to be glued to the cylinder ends. Computations with no temperature perturbation introduced at the center showed that a shear band initiated from the top right corner and propagated inward when sticking friction was considered, but no such localization effects were observed when the contact surfaces were taken to be smooth.

That the localization of deformation is significantly delayed for the axisymmetric problem with no friction is evidenced by the plot in Fig. 4(a) of the evolution of the second invariant I of

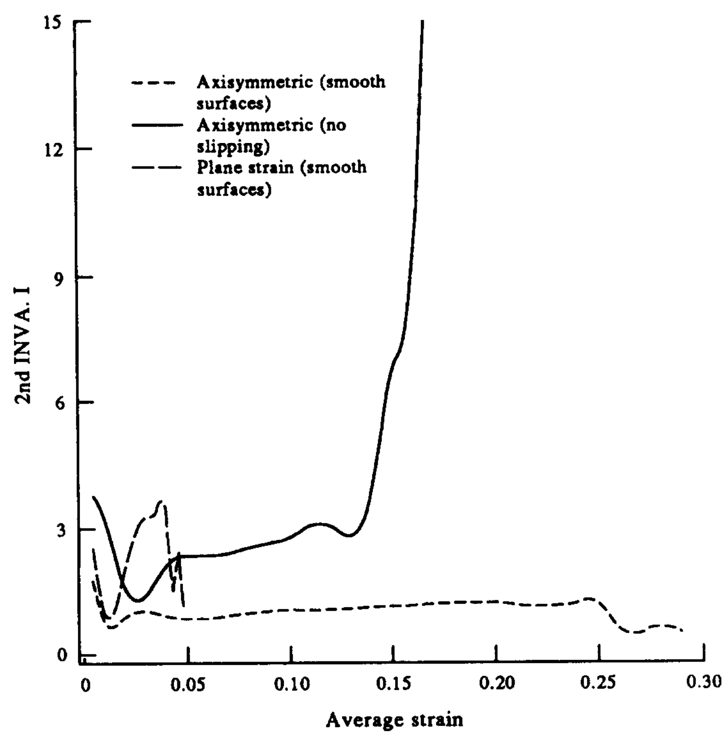

Fig. 3. Evolution of the second invariant of the deviatoric strain-rate tensor at the top right corner.

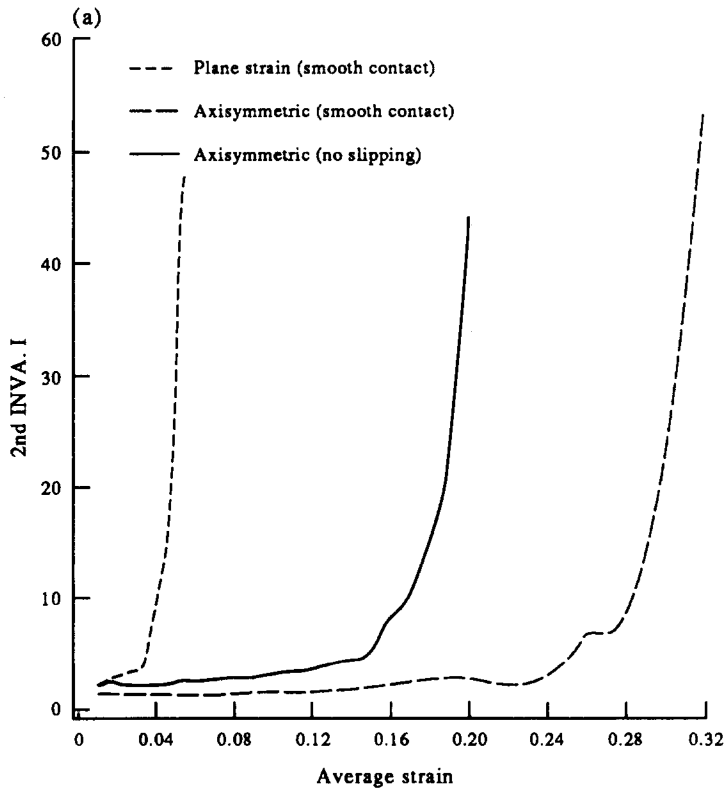

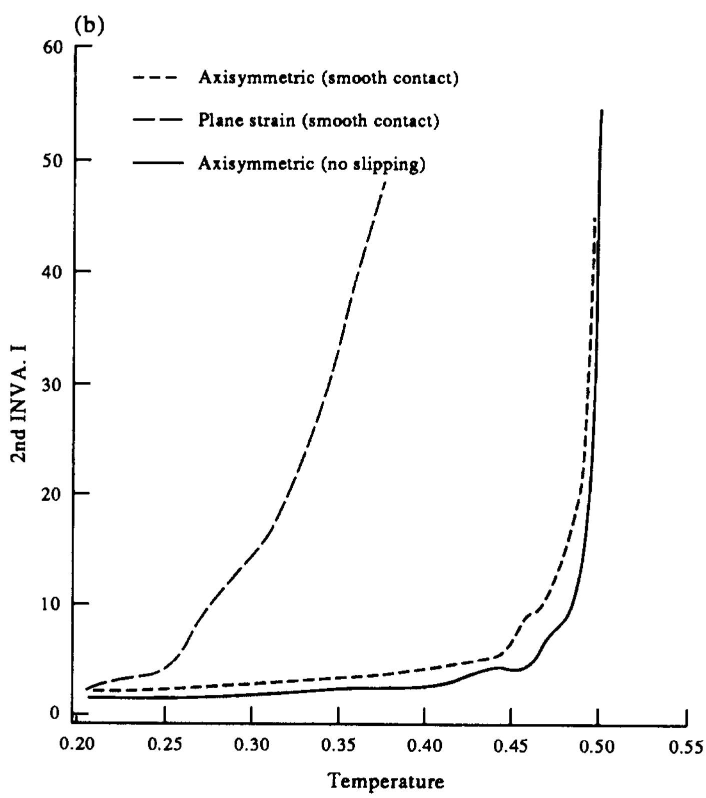

Fig. 4. (a) Evolution of the second invariant of the deviatoric strain-rate tensor at the centroid of the cylinder; (b) variation of the second invariant of the deviatoric strain-rate tensor at the cylinder center with the temperature there.

the deviatoric strain-rate tensor at the centroid of the cylinder. We have also included the corresponding result for the case when a cylindrical body of square cross-section (10 × 10 mm) and made of the material of the circular cylinder studied herein is deformed in plane strain compression at an average strain-rate of 5000 s^{-1}. It is transparent from these plots that the rapid increase in the values of I occurs at the lowest value of the average strain when the body is deformed in plane strain compression and at the highest value of the average strain when the deformations are axisymmetric and the contact surfaces are smooth. Also, during the time I increases rapidly, its rate of increase seems to be the least for axisymmetric deformations with smooth surfaces. However, when I at the cylinder center is plotted against the temperature there [cf. Fig. 4(b)] the effect of boundary conditions at the end faces is minimal. Since the temperature at the cylinder center increases monotonically until the material there melts, the abscissa represents a distorted time scale.

(a)

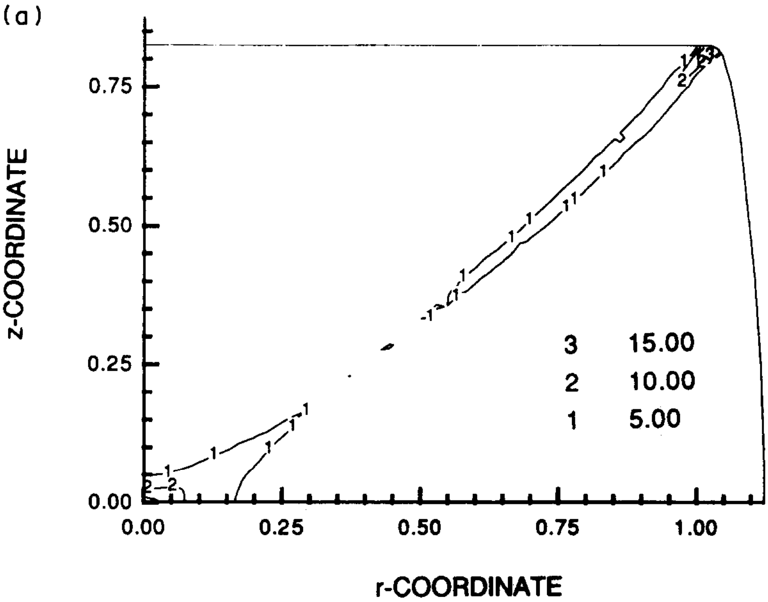

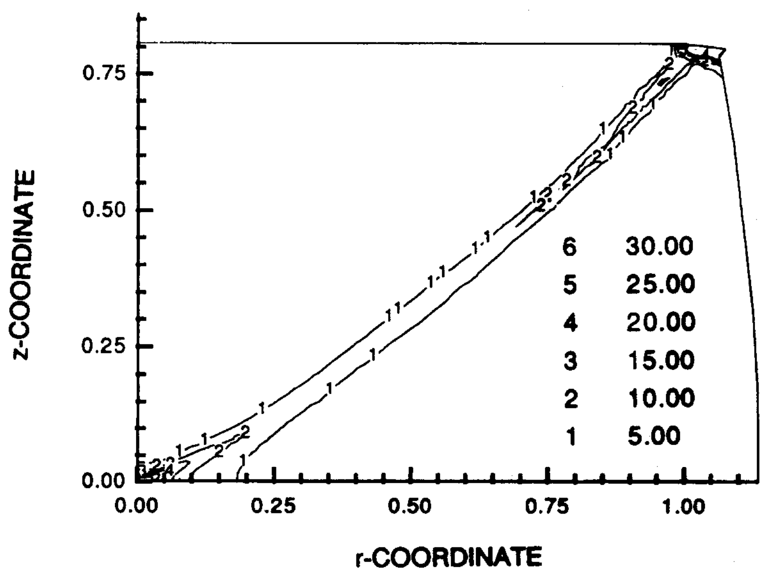

Fig. 5.—(*Caption overleaf*).

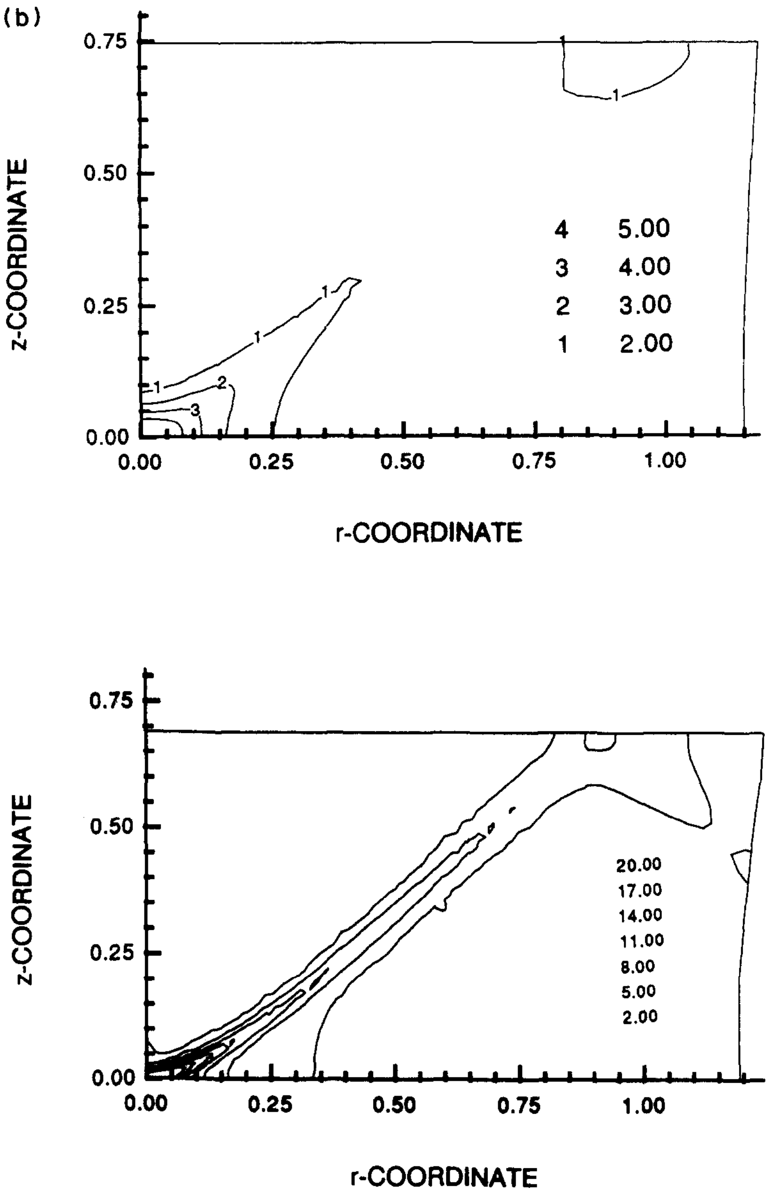

Fig. 5. Contours of the second invariant of the deviatoric strain-rate tensor at two different times: (a) no slipping—$t = 0.180$, 0.197; (b) smooth contact—$t = 0.260$, 0.315.

The contours of the second invariant I of the deviatoric strain-rate tensor at two different times are plotted in Fig. 5(a) for the case of no sliding between the cylinder ends and the loading device, and in Fig. 5(b) for the case of smooth contact. In each case the contours of increasingly higher values of I originate at points where the deformation localizes first and propagate outward. By estimating the distance through which the ends of the contour have diffused out and the time taken to do so, we determine the speed of propagation of the contour of $I = 10$ to be 216 m/s for the one originating at the center and 389 m/s for that initiating at the top right corner. However, when the cylinder ends are taken to be smooth, the contour of $I = 10$ propagates at 313 m/s. We note that Marchand and Duffy [2] estimated the tentative speed of a shear band to be either 255 or 510 m/s depending upon whether or not it propagated in both directions around the specimen circumference. The rather good match between the computed speeds and those given by Marchand and Duffy, while gratifying, is really illusive since the speed of propagation of the shear band depends upon the state of deformation within and around it. We have not established any such correlation between the computed deformation field and that observed experimentally. We should study a 3-dimensional problem in order to accomplish this.

Figure 6 exhibits contours of temperature at two different times for the two cases studied herein. For the case of sticking surfaces, the temperature at the top right corner is comparable to that at the cylinder center, even though the initial temperature at the center is considerably higher that that at the top right corner. It suggests that the deformations of the region near the top right corner are more intense than those of the material near the center of the cylinder.

The distribution at different times of the second invariant I of the deviatoric strain-rate tensor at points on the horizontal centroidal axis is depicted in Fig. 7. It is clear that the severely deforming region adjoining the centroid of the cylinder becomes narrower as the cylinder continues to be compressed. That the intense deformations are confined to a somewhat narrow band is evidenced by the plots, given in Fig. 8, of the normalized effective stress, temperature, and the second invariant I of the deviatoric strain-rate tensor, at the final time considered, on lines AB and CD perpendicular to the estimated centerline of the shear

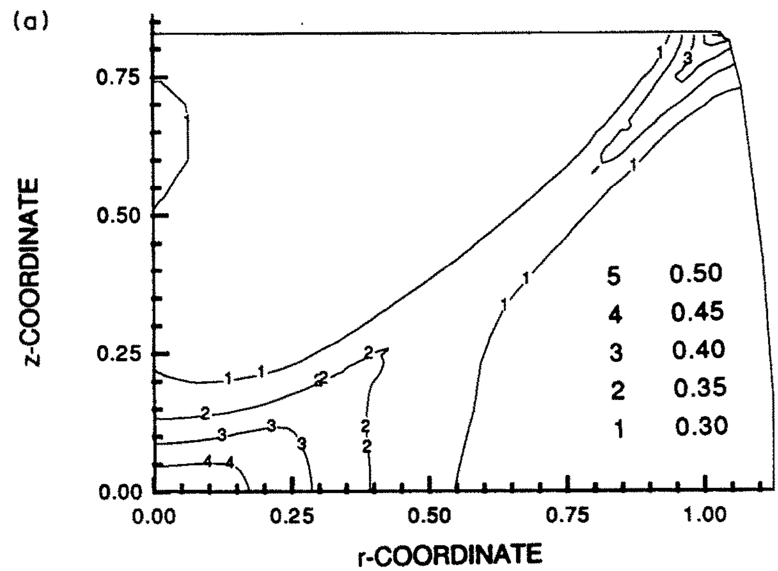

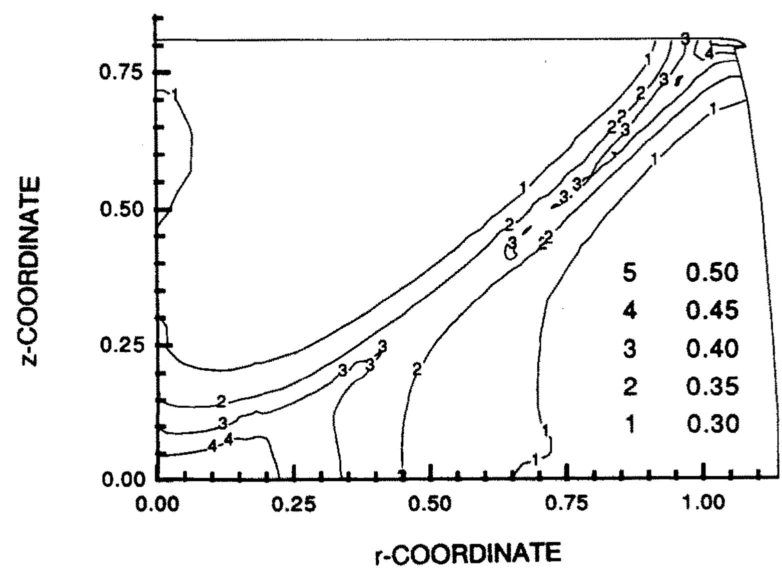

Fig. 6.—(*Caption overleaf*).

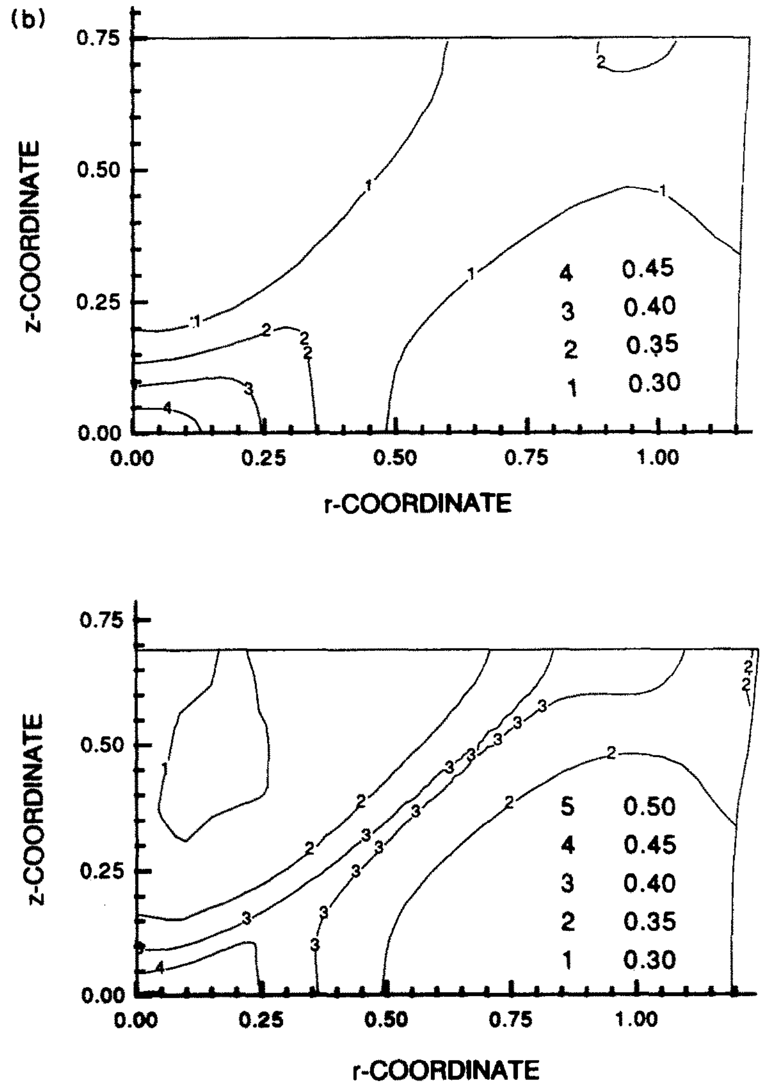

Fig. 6. Contours of the temperature at two different times: (a) no slipping—$t = 0.180$, 0.197; (b) smooth contact—$t = 0.260$, 0.315.

band. A quantity is normalized with respect to its peak value at points on AB or CD, and the abscissa equals the distance of a point from A or C. The centerline of the shear band was determined from the contours of the second invariant I of the deviatoric strain-rate tensor, and was assumed to be made up of two line segments for the case of smooth contacting surfaces, and three line segments when the contact surfaces are rough. These lines are shown in the insert in Fig. 8. Note that the centerline of the band changes with time, which inhibits depicting results using 3-dimensional graphics. The plots in Fig. 8 suggest that a narrow region around the points of intersection of lines AB and CD with the centerline of the band, undergoes intense deformations. The nondimensional effective stress, s_e, is defined as

$$s_e = \left(\frac{1}{2}\operatorname{tr}(\mathbf{s}\mathbf{s}^T)\right)^{1/2} = \frac{1}{\sqrt{3}}(1 + bI)^m(1 - \nu\theta). \tag{16}$$

Its lower values at points close to the centerline of the band indicate that thermal softening there exceeds the strain-rate hardening.

The variation of the normalized values of the second invariant of the deviatoric strain-rate tensor, effective stress, and the temperature along the estimated centerline of the band, shown in Fig. 9, indicates that only a narrow region near the center of the cylinder is undergoing

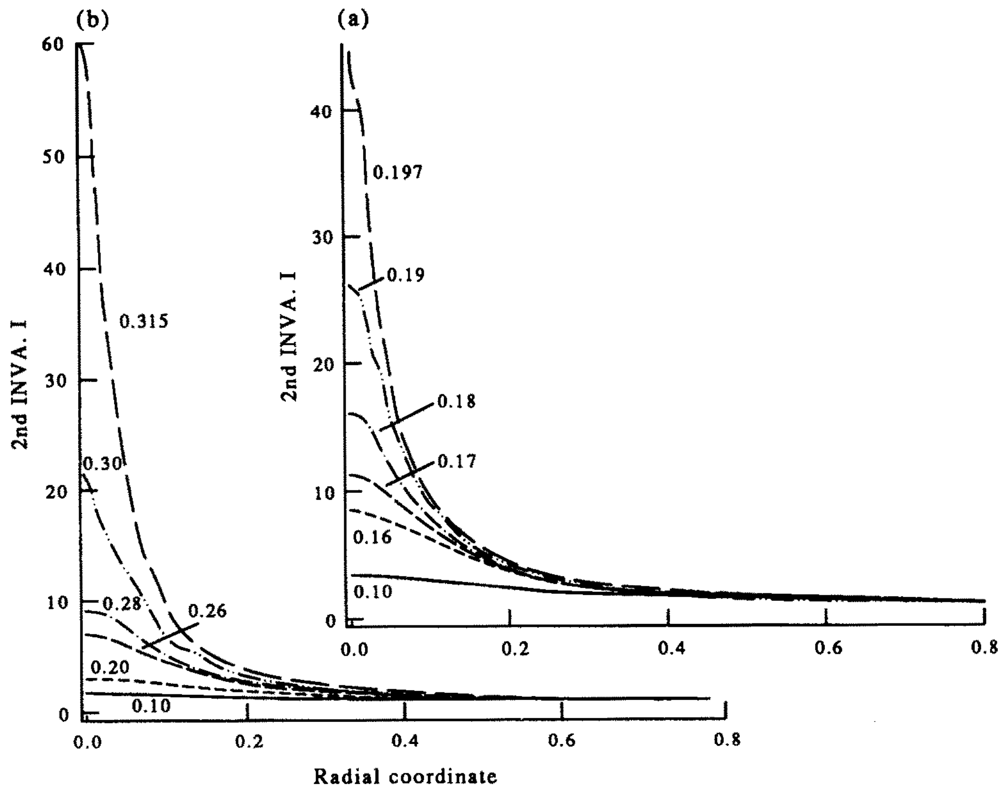

Fig. 7. Variation of the second invariant of the deviatoric strain-rate tensor on the centroidal axis at different times; the time is indicated on the curves: (a) no slipping; (b) smooth contact.

intense deformations. When frictional forces are accounted for, the material near the top right corner is also deforming severely. In this case, the second invariant of the deviatoric strain-rate tensor is higher near the top right corner than that at the cylinder centroid. We note that as the cylinder is compressed different material particles on the mantle of the cylinder contact the loading surface; thus, a new material particle is situated at the top right corner as time varies. Since the temperature rise at a point is a measure of the total energy dissipated there, less energy has been dissipated at points on the centerline of the band that are away from the corners. We stopped the computations as soon as a material point melted. Even though the material there failed, the surrounding material provides strength to the structure and the cylinder can still be compressed further. However, in view of the limited computational resources available to us, this was not attempted.

Figure 10 exhibits the variation with average strain of the average normal traction f_n and the average tangential traction f_t acting on the top surface. These are defined as

$$f_n = -\frac{1}{r_0^2}\int_0^{r_0} \sigma_{zz}(r, \bar{z})r\,dr, \qquad f_t = \frac{1}{r_0^2}\int_0^{r_0} \sigma_{rz}(r, \bar{z})r\,dr, \tag{17}$$

where r_0 is the radius of the cylinder in the deformed configuration. For the case of smooth surfaces f_n decreases gradually, but for the frictional case the transients seem to persist during the entire duration of the simulation. We note that the integrands in equation (17) are evaluated at points on the top surface for which $z = \bar{z}$, and the abscissa in Fig. 10 is proportional to the vertical displacement of the top surface. For the case of rough surfaces, the temperature of material particles adjoining the top surface rises noticeably soon after the load is applied, thus making the material there softer and easier to deform. This accounts for the sharp decrease in the average normal traction required to compress the cylinder at the prescribed rate. Because of the increase in the value of r_0 with time, the variation of the

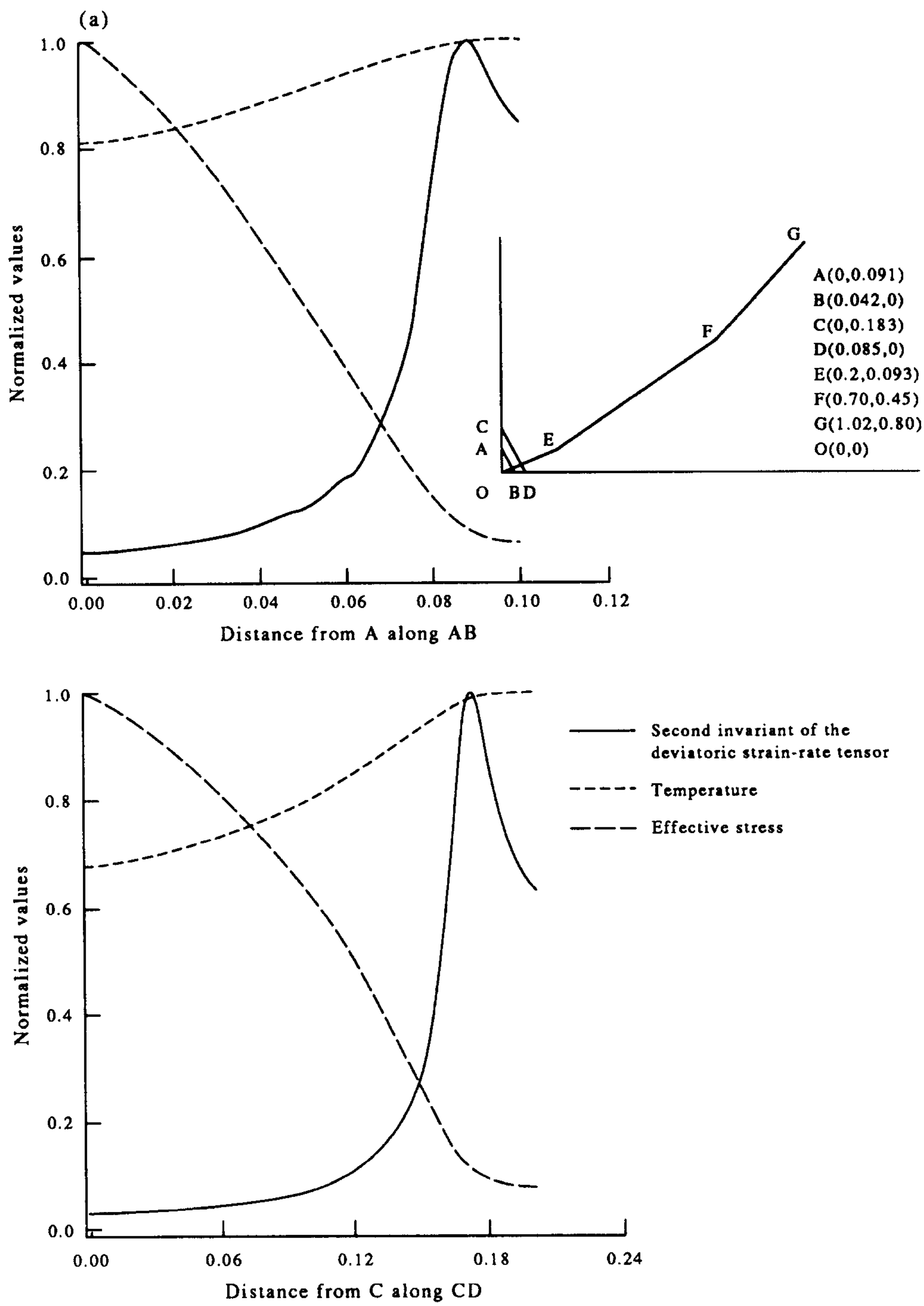

Fig. 8.—(*Caption overleaf*).

total load acting on the top surface with time will be different from that of f_n. It is interesting to see that the average tangential traction on the top cylinder end exceeds the average normal traction there and the two are out of phase with each other, implying thereby that f_t is not proportional to f_n. For the body deformed in plane strain compression, the average normal traction on the top surface is a little less than that for the same body undergoing axisymmetric deformations.

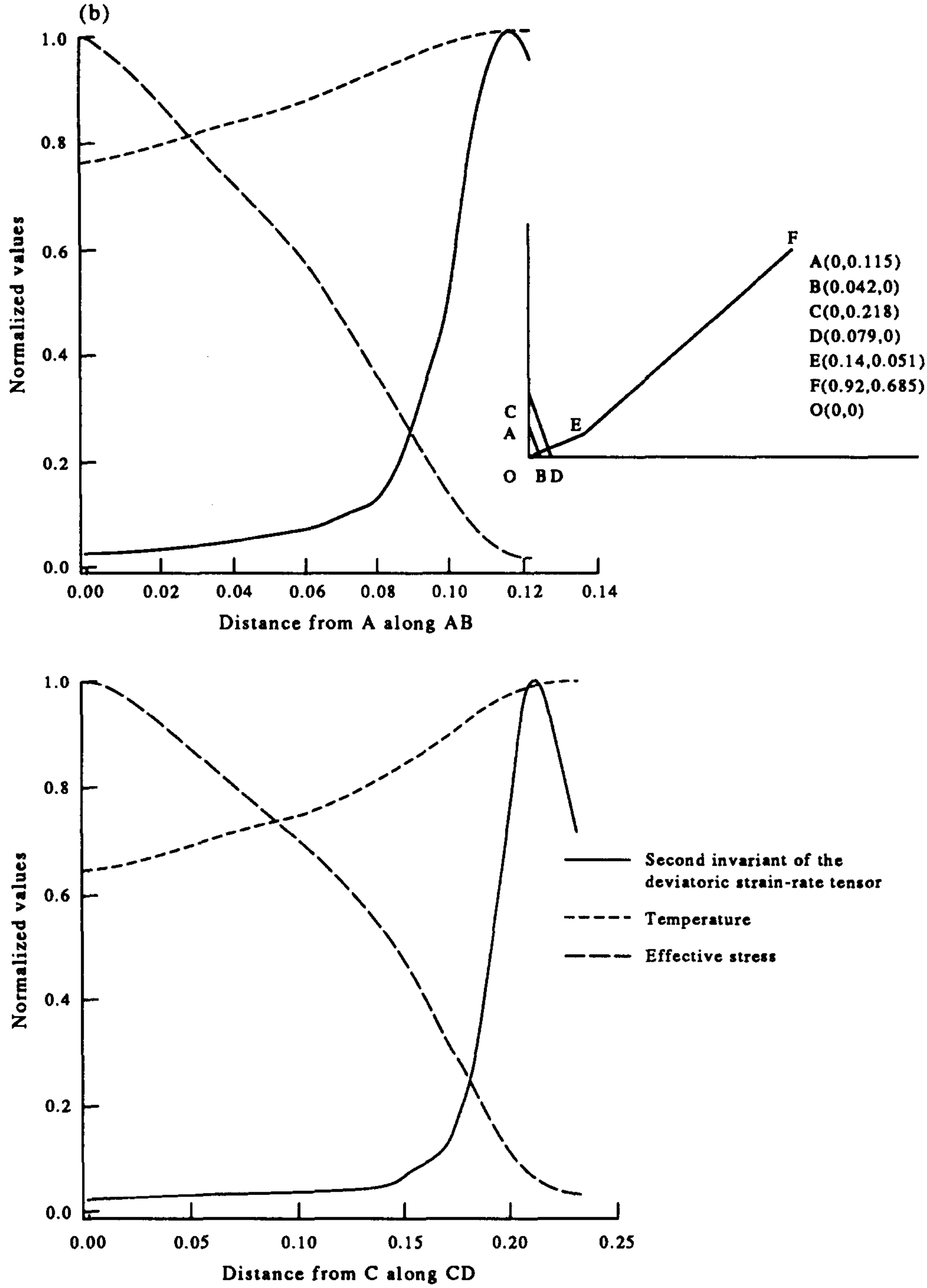

Fig. 8. Variations, at the final time considered, of the normalized effective stress, temperature, and the deviatoric strain-rate tensor on two lines perpendicular to the estimated centerline of the shear band: (a) no slipping; (b) smooth contact.

5. CONCLUSIONS

We have studied the initiation and growth of shear bands in a thermally softening viscoplastic cylindrical body compressed at a nominal strain-rate of $5000\,s^{-1}$. It is presumed that its deformations stay axisymmetric even after a shear band has formed. The loading device can either slide freely on the cylinder end, or does not slide at all. A shear band forms sooner when frictional effects are considered than when they are not. Also, a comparison of the presently computed results with those for the same body deformed in plane strain compression reveals

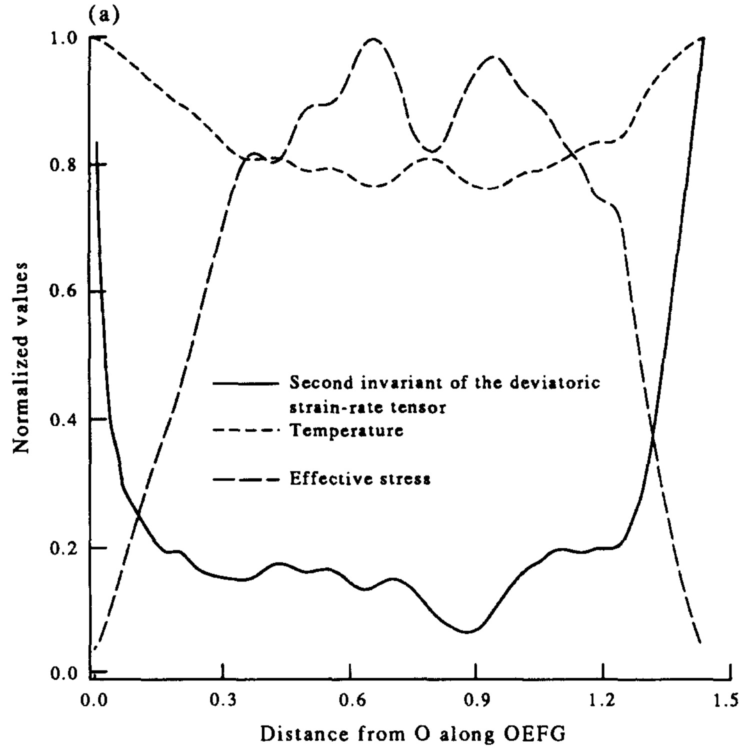

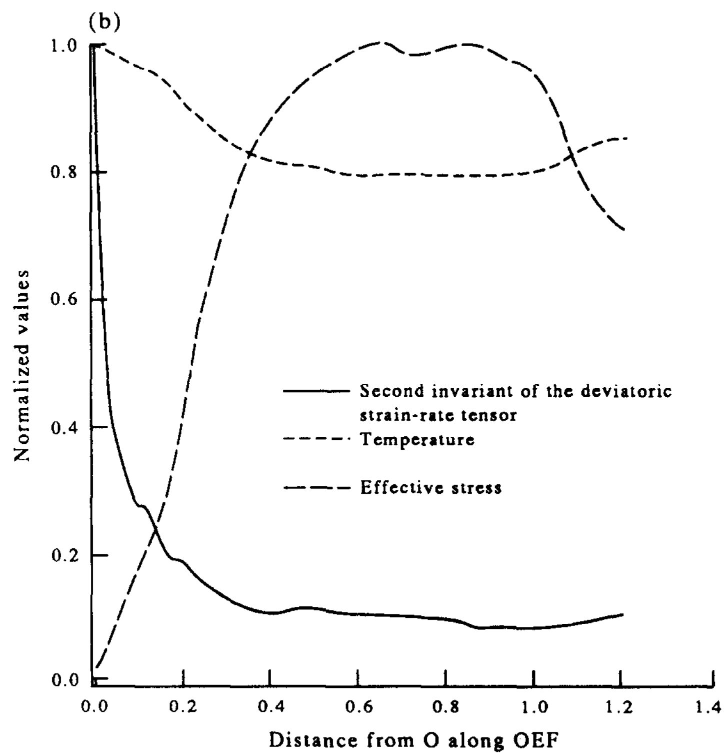

Fig. 9. Variation, at the final time considered, of the normalized effective stress, temperature, and the deviatoric strain-rate tensor on the estimated centerline of the shear band: (a) no slipping; (b) smooth contact.

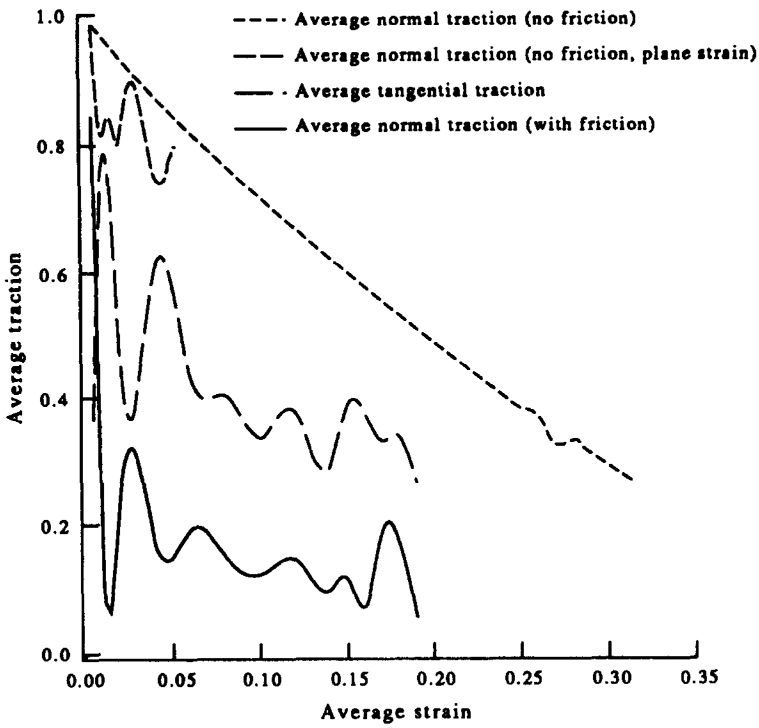

Fig. 10. Variation with time of the average normal and tangential tractions acting on the cylinder ends.

that the initiation of a shear band is significantly delayed in the body undergoing axisymmetric deformations. For the case of no slipping, the strain-rate at the top right corner also increases significantly, and it equals or exceeds that at the center of the cylinder. The defo.med shape of the cylinder looks like a barrel when the loading surface is assumed to be glued to the cylinder end, and like a reversed barrel when the surfaces can slide freely over each other. This agrees qualitatively with the experimental findings. The average tangential traction required to prevent sliding of the loading surface over the cylinder end exceeds the average normal traction there, and the two are out of phase with each other.

Acknowledgements—This work was supported by the U.S. Army Research Office grant DAAL03-91-G-0084 and the U.S. NSF grant MSS9121279 to the University of Missouri-Rolla. Some of the computations were performed on the NSF sponsored supercomputer center in Ithaca, New York.

REFERENCES

[1] C. ZENER and J. H. HOLLOMON, *J. Appl. Phys.* **14,** 22 (1944).
[2] A. MARCHAND and J. DUFFY, *J. Mech. Phys. Solids* **36,** 251 (1988).
[3] J. H. GIOVANOLA, *Mech. Mater.* **7,** 73 (1988).
[4] T. W. WRIGHT and J. W. WALTER, *J. Mech. Phys. Solids* **35,** 701 (1987).
[5] R. C. BATRA and C. H. KIM, *J. Mech. Phys. Solids* **38,** 859 (1990).
[6] R. C. BATRA, *Int. J. Plasticity* **3,** 75 (1987).
[7] M. E. BACKMAN and S. A. FINNEGAN, The propagation of adiabatic shear. In *Metallurgical Effects at High Strain-Rates* (Edited by R. W. RHODE *et al.*), pp. 531–543. Plenum Press, New York (1973).
[8] G. L. WULF, *Int. J. Mech. Sci.* **20,** 609 (1978).
[9] J. LITONSKI, *Bull. Acad. Poloinaise Sci.* **25,** 7 (1977).
[10] R. C. BATRA, *Comput. Mech.* **3,** 1 (1988).
[11] R. C. BATRA and R. JAYACHANDRAN, *Int. J. Impact Engng.* **12,** 209 (1992).
[12] S. R. BODNER and Y. PARTOM, *J. Appl. Mech.* **42,** 385 (1975).
[13] S. B. BROWN, K. H. KIM and L. ANAND, *Int. J. Plasticity* **5,** 95 (1989).
[14] J. F. BELL, *Physics of Large Deformation of Crystalline Solids.* Springer, New York (1968).
[15] M. R. LIN and R. H. WAGONER, *Scripta Metall.* **20,** 143 (1986).

[16] U. S. LINDHOLM and G. R. JOHNSON, Strain-rate effects in metals at large strain rates. In *Material Behaviour Under High Stresses and Ultrahigh Loading Rates* (Edited by J. MESCAL and V. WEISS), pp. 61–79. Plenum Press, New York (1983).
[17] A. C. HINDMARSH, ODEPACK, a systematized collection of ODE solvers. In *Scientific Computing* (Edited by R. S. STEPLEMAN *et al.*), pp. 55–64. North-Holland, Amsterdam (1983).
[18] R. C. BATRA and K. I. KO, *Comput. Mech.* In press (1993).
[19] G. L. WULF, *Int. J. Mech. Sci.* **21,** 713 (1979).
[20] S. CESCOTTO and D. W. ZHOU, *Commun. Appl. Numer Meth.* **5,** 473 (1989).
[21] S. H. LO, *Int. J. Numer. Meth. Engng* **21,** 1403 (1985).
[22] J. PERAIRE, M. VAHDATI, K. MORGAN and O. C. ZIENKIEWICZ, *J. Comp. Phys.* **72,** 449 (1987).
[23] J. PERAIRE, J. PEIRO, L. FORMAGGIA, K. HORGAN and O. C. ZIENKIEWICZ, *Int. J. Numer. Meth. Engng* **26,** 2135 (1988).
[24] A. M. HABRAKEN and S. CESCOTTO, *Int. J. Numer. Meth. Engng* **30,** 1503 (1990).
[25] R. LÖHMER, *Commun. Appl. Meth.* **4,** 123 (1988).

APPENDIX

At the referee's suggestion, we describe below the adaptive mesh refinement technique; the material is taken from Ref. [18], wherein results, including error norms, for adaptively refined meshes for a plane strain problem are compared with those obtained with a fixed mesh.

We first select a coarse mesh and find a solution of the problem formulated in Section 2. This mesh is refined so that

$$a_e = \int_{\Omega_e} I \, d\Omega, \qquad e = 1, 2, \ldots, n_{e1}, \tag{A1}$$

is nearly the same for each element Ω_e. In (A1), n_{e1} equals the number of elements in the coarse mesh and Ω_e is one of the elements. Since one may not have an idea where the solution will exhibit sharp gradients, we choose the coarse mesh to be uniform. The motivation behind making a_e the same over each element Ω_e is that within the region of localization of the deformation values of I are very high as compared to those in the remaining region. Other variables such as the temperature rise, the maximum principal strain, and the equivalent strain which are also quite large within the band will be suitable replacements for I in equation (A1). The refined mesh will depend upon the variable used in equation (A1). In order to refine the mesh, we find

$$\bar{a} = \frac{1}{n_{e1}} \sum_{e=1}^{n_{e1}} a_e, \tag{A2}$$

$$\xi_e = \frac{a_e}{\bar{a}}, \tag{A3}$$

$$h_e = \frac{\bar{h}_e}{\xi_e}, \tag{A4}$$

and

$$H_n = \frac{1}{N_e} \sum_{e=1}^{N_e} h_e, \qquad n = 1, 2, \ldots, n_{od}. \tag{A5}$$

Here, $\bar{h}_e$ is the size of the element Ω_e in the coarse mesh, N_e equals the number of elements meeting at node n, and n_{od} equals the number of nodes in the coarse mesh. We refer to H_n as the nodal element size at node n.

In order to generate the new mesh, we first discretize the boundary by following the procedure given by Cescotto and Zhou [20]. Let AB be a segment of the contour to be discretized, s the arc length measured from point A, and H_A and H_B be nodal element sizes for nodes located at points A and B, respectively. From a knowledge of the values of H at discrete points, corresponding to the nodes in the coarse mesh, on AB we define a piecewise linear continuous function $H(s)$ that takes the previously computed values at the node points. In order to discretize AB for the new mesh, we start from point A, if $H_A < H_B$; otherwise we start from B. For the sake of discussion, let us assume that A is the starting point. We first find temporary positions of nodes on the segment AB by using the following recursive procedure. Assume that points $1, 2, \ldots, k$ have been found. Then the temporary location of point $(k+1)$ is given by

$$s_{k+1} = s_k + \frac{1}{2}[H(s_k) + H(s^*_{k+1})], \tag{A6}$$

where

$$s^*_{k+1} = s_k + H(s_k). \tag{A7}$$

Referring to Fig. A1, the above procedure will give rise to the following four alternatives: $a = b = 0$, $a < b$, $a > b$, $a = b \neq 0$. If $a = b = 0$, then the temporary locations of node points are their final positions. Depending upon whether

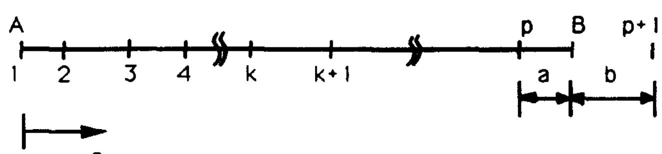

Fig. A1. Discretization of a boundary segment for mesh refinement.

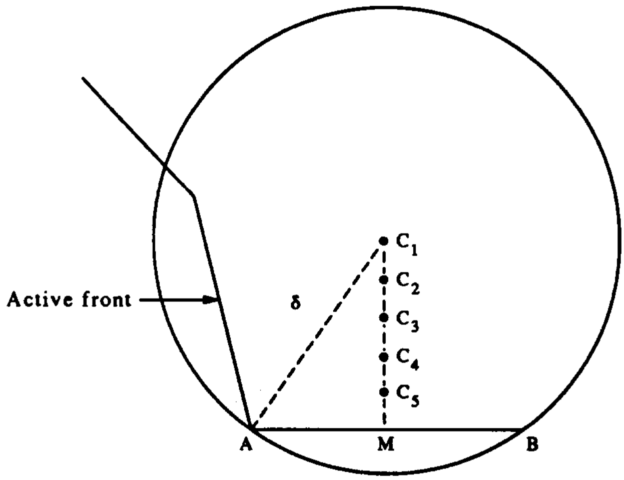

Fig. A2. Advancing front and new element generation.

$a < b$ or $b \leq a$, the node points 2 to p or 2 to $p+1$ are moved, the displacement of a node being proportional to the value of H there, so that either node p or node $(p+1)$ coincides with B. This determines the final positions of nodes on the segment AB.

Having discretized the boundary, we use the concept of advancing front (e.g. see Lo [21], Peraire *et al.* [22, 23], and Habraken and Cescotto [24]) to generate the elements. An advancing front consists of straight line segments which are available to form a side of an element. Thus, to start with, it consists of the discretized boundary. We choose the smallest line segment (say side AB) connecting the two adjoining nodes, and determine the nodal element size $H_M \equiv H(s_M) = (H_A + B_B)/2$ at the midpoint M of AB. We set

$$\delta = \begin{cases} 0.8\overline{AB} & \text{if } H_M < 0.8\overline{AB}, \\ H_M & \text{if } 0.8\overline{AB} \leq H_M \leq 1.4\overline{AB}, \\ 1.4\overline{AB} & \text{if } 1.4\overline{AB} < H_M, \end{cases} \tag{A8}$$

and find point C_1 at a distince δ from A and B (cf. Fig. A2). Here $\overline{AB}$ equals the length of segment AB. We search for all nodes on the active front that lie inside the circle with center at C_1 and radius δ, and order them according to their distance from C_1 with the first node in the list being closest to C_1. At the end of this list are added points C_1, C_2, C_3, C_4, and C_5, which lie on C_1M and divide it into five equal parts. We next determine the first point C in the list that satisfies the following three conditions.

(i) Area of triangle $ABC > 0$.

(ii) Sides AC and BC do not cut any of the existing sides in the front.

(iii) If any of the points $C_1, C_2, \ldots, C_5$ is chosen, that point is not too close to the front. The triangle ABC is an element in the new mesh. If C is one of the points $C_1, C_2, \ldots, C_5$, then a new node is also created. The advancing front is updated by removing the line segment AB from it, and adding line segments AC and CB to it. The element generation process ceases when there is no side left in the active front.

We determine the values of solution variables at a newly created node by first finding out to which element in the coarse mesh this node belongs, and then finding values of solution variables at this node by interpolation. This process and that of searching for line segments and points in the aforestated element generation technique consume a considerable amount of CPU time. These operations are optimized to some extent by using the heap list algorithm (e.g. see Löhmer [25]) for deleting and inserting new line segments, and quadtree structures and linked lists for searching line segments and points and also for the interpolation of solution variables at the newly created nodes.

(Revision received 3 May 1992; accepted 7 July 1992)